Defence Research and Development Canada
Recherche et développement pour la défense Canada

DEFENCE R&D DÉFENSE

Advanced materials for soldier power applications through waste-heat recovery:

Final report

Gisele Amow
DRDC Atlantic

Defence Research and Development Canada – Atlantic

Technical Report
DRDC Atlantic TR 2009-213
September 2009

Canada

Advanced materials for soldier power applications through waste-heat recovery:

Final report

Gisele Amow
DRDC Atlantic

Defence Research and Development Canada – Atlantic

Technical Report

DRDC Atlantic TR 2009-213

September 2009

Principal Author

Original signed by G. Amow

G. Amow

Defence Scientist/Air Vehicle Research Section

Approved by

Original signed by Ken McRae

Ken McRae

Section Head/Air Vehicle Research Section

Approved for release by

Original signed by Calvin Hyatt

Calvin Hyatt

Chair Document Review Panel/DRDC Atlantic

Land Sustain Thrust 12sz

Abstract

With the ever increasing power demands required for the dismounted soldier, ongoing efforts have been underway to identify alternatives to battery use. Emerging technologies such as fuel cells show promise for increased power densities and thus have the potential for reducing footprint and enabling longer mission times, whilst thermoelectric devices can convert the waste heat into useable power from various sources such as that produced by fuel cells and natural body heat.

This report describes the most significant results of a three year Technology Investment Fund (TIF) project focused on addressing materials issues related to solid-oxide fuel cells and thermoelectric materials. Namely, the development of a novel porous electrolyte supported solid oxide fuel cell (SOFC) architecture and the development of novel materials for SOFC cathodes, thermoelectric oxides and polymers.

Résumé

En raison des demandes de puissance électrique de plus en plus grandes pour l'infanterie débarquée, on continue de déployer des efforts dans le but de trouver des solutions de remplacement aux piles. Certaines technologies émergentes, comme les piles à combustible, s'avèrent intéressantes pour obtenir une densité de puissance accrue et ont, par le fait même, le potentiel de réduire l'empreinte et d'effectuer des missions plus longues; les dispositifs thermoélectrique peuvent, quant à eux, convertir la chaleur dissipée en puissance utilisable à partir de différentes sources, comme la chaleur produite par les piles à combustible et la chaleur naturelle du corps.

Le présent rapport décrit les résultats les plus significatifs d'un projet de Fonds d'investissement technologique (FIT) d'une durée de trois ans. Le projet portait sur des questions pratiques liées aux piles à combustible à oxyde solide (SOFC, de l'anglais *Solid Oxide Fuel Cell*) et aux matériaux thermoélectriques. Plus précisément, on procédera à l'élaboration d'une nouvelle architecture de pile à combustible à oxyde solide à support électrolytique poreux et de nouveaux matériaux pour les cathodes de SOFC, les oxydes thermoélectriques et les polymères.

This page intentionally left blank.

Executive summary

Advanced materials for soldier power applications through waste-heat recovery: Final report

G. Amow; DRDC Atlantic TR 2009-213; Defence R&D Canada – Atlantic; September 2009.

Introduction or background: Today's dismounted soldiers must carry with them an ever-increasing number of electronics for operational and information gathering purposes. Alone, these devices can easily add up to 100 pounds of gear. To power them, soldiers can count on carrying significant amount of weight in batteries of various types. These problems are inherent to the limited power capacity batteries offer. Primary batteries are one-shot use while rechargeable batteries are costly and require burdensome backup power supplies. As such, it is necessary to consider alternative power technologies to decrease the logistic burden while at the same time ensuring mission effectiveness. The use of energy conversion systems, such as fuel cells and thermoelectric generators, to replace or complement battery-use could resolve some of the weight and power capacity problems presented by batteries. Furthermore, recognizing that solid-oxide fuel cells are high temperature devices, and that thermoelectric devices convert heat into power, it seems natural to hybridize these two technologies for even greater efficiencies by harvesting the waste heat produced from the fuel cell into useable power.

The goal of this project was to develop a novel solid oxide microtubular architecture to mitigate the problems associated with redox cycling, as well as to develop new materials for solid-oxide fuel cell cathodes, thermoelectric oxides and polymers to someday enable a fuel-cell thermoelectric hybrid system or power generation from body heat with *'smart'* clothing.

Results: A novel solid oxide fuel cell architecture was developed with a porous electrolyte support design. Electrochemical testing of a four cell stack indicates good long term stability relative to the conventional anode-supported design. Some limited advancements were also made with the materials development of solid oxide fuel cell cathodes, thermoelectric oxides and polymers; with the latter demonstrated to have good thermal stability for the first time.

Significance: The defence potential for this work is promising. Used alone or in a hybrid system, both these technologies are viable considerations for decreasing the logistic burdens (size, weight, mission lifetimes etc.) associated with current battery technologies.

Future plans: Given the success of this project to establish core competencies in fuel cells and thermoelectrics, it is recommended that materials research and development be continued in these areas. However, there are no immediate plans to develop Alberta Research Council's fuel cell stack, thermoelectric oxides and polymers, as the high-risk associated with these activities limit the funding avenues for immediate follow-on plans. In addition to the developed core competencies in fuel cells and thermoelectrics, another core competency in microcogeneration (simultaneous production of heat and power) has also been established. Follow-on activities include the evaluation of a 25W SOFC portable unit and a 1 kW microcogeneration PEMFC system, which are currently underway.

Sommaire

Advanced materials for soldier power applications through waste-heat recovery: Final report

G. Amow; DRDC Atlantic TR 2009-213; R & D pour la défense Canada – Atlantique; Septembre 2009.

Introduction : Aujourd'hui, les soldats débarqués doivent transporter avec eux un nombre toujours croissant de dispositifs électroniques utilisés à des fins opérationnelles et de collecte d'information. À eux seuls, ces dispositifs peuvent facilement représenter jusqu'à cent livres d'équipement. Pour les alimenter, les soldats peuvent s'attendre à transporter un poids important de piles de divers types. La capacité de puissance offerte par ces piles est limitée. Les piles primaires sont des piles à une seule utilisation, alors que les piles rechargeables sont coûteuses et exigent une alimentation de secours coûteuse. Pour cette raison, il est nécessaire d'envisager le recours à des technologies de puissance de remplacement afin de réduire la charge logistique tout en assurant l'efficacité de la mission. L'utilisation de systèmes de conversion de l'énergie, comme les piles à combustible et les générateurs thermoélectriques pour remplacer ou compléter l'utilisation de piles pourrait permettre de résoudre certains des problèmes de masse et de capacité de puissance qui y sont associés.

Bien que les principes de fonctionnement des piles à combustible et des générateurs thermoélectriques soient connus depuis le début du XIX^{e} siècle, des problèmes matériels ont empêché leur succès commercial. Dans le cas des piles à combustible, les problèmes de durabilité et d'alimentation n'ont pas encore été résolus tandis que dans le cas des générateurs thermoélectriques, une très faible efficacité de conversion est la norme. Le but du présent projet a été de réaliser des progrès importants dans les propriétés que doivent posséder les matériaux pour ouvrir la voie à l'hybridation future de ces deux technologies, par exemple un système hybride constitué d'une pile à combustible et d'un générateur thermoélectrique, ou un système d'alimentation électrique à partir de la chaleur corporelle utilisant des vêtements « *intelligents* » à générateurs thermoélectriques.

Résultats : On a mis au point un nouveau type de pile à combustible à oxyde solide à électrolyte-support poreux. Des essais électrochimiques portant sur un assemblage de quatre piles ont indiqué une bonne stabilité à long terme par rapport aux piles à anode-support classiques. On a également réalisé des progrès limités en ce qui a trait à l'élaboration de matériaux de cathodes pour piles à combustible à oxyde solide, de polymères et d'oxydes thermoélectriques, ceux-ci ayant démontré une bonne stabilité thermique pour la toute première fois.

Portée : Le potentiel de ces travaux est fort intéressant sur le plan de la défense. Employées seules, ou dans des systèmes hybrides, ces deux technologies constituent des solutions viables permettant de réduire la charge logistique associée aux technologies actuelles utilisant des piles.

Recherches futures : Étant donné que le succès de ce projet dépend de l'établissement de compétences essentielles dans le domaine des piles à combustible et des dispositifs thermoélectriques, il est recommandé que la recherche et le développement sur les matériaux se poursuive dans ce domaine. Cependant, il n'y a pas de plans immédiats visant à mettre au point un assemblage de piles à combustible pour l'Alberta Research Council, des polymères et des

oxydes thermoélectriques, étant donné que les risques élevés associés à ces activités limiteront les possibilités de financement relatives aux plans de suivi dans l'immédiat. En plus des compétences de base associées aux piles à combustible et aux dispositifs thermoélectriques, une autre compétence essentielle a été établie en ce qui a trait à la microcogénération (production simultanée de chaleur et de puissance). Les activités de suivi comprennent l'évaluation d'une unité portative SOFC de 25 W et un système PEMFC de microcogénération de 1 kW, qui sont actuellement en cours d'élaboration.

This page intentionally left blank

Table of contents

List of figures

List of tables

Acknowledgements

This project was funded by the DRDC Technology Investment Fund. The author thanks the Alberta Research Council, Université Laval and the University of Waterloo for their participation and contributions to this project.

1 Introduction

1.1 Background

Today's dismounted soldiers must carry with them an ever-increasing number of electronics for operational and information gathering purposes. Alone, these devices can easily add up to 100 pounds of gear. To power them, soldiers can count on carrying up to a third of their body weight in batteries and even more if extended missions are required. These problems are inherent to the limited power capacity batteries offer. Primary batteries are one-shot use while rechargeable batteries are too costly and require burdensome backup power supplies. The use of energy conversion systems, such as fuel cells and thermoelectric generators, to replace or complement battery-use could resolve some of the weight and power capacity problems that batteries present.

Fuel cells are electrochemical devices that convert chemical energy into electrical energy and can do so indefinitely so long as fuel is continuously supplied to the system. The advantages of fuel cells to the military include sustained increased power densities, low noise signatures and associated environmental benefits with water and high-quality heat as by-products. Furthermore, typical efficiencies are higher than that for internal combustion engines (45-55% with no heat recovery). The solid-oxide fuel cell (SOFC) system has been primarily targeted for stationary applications, such as auxiliary power units (APUs) because of their potential to operate on logistical fuels. However, the high thermal mass, low thermal shock resistance, and relatively long start-up times of minutes of the planar-based SOFCs make them undesirable for portable applications. With the microtubular fuel cell architecture, SOFC technology could perceivably be adapted for portable applications where moderate power demands are required. Quick start-up times (minutes) can be facilitated by the increased thermal shock resistance afforded by this design **[1]**.

By contrast, thermoelectric generators (TG) convert heat energy into electrical energy by the Seebeck effect **[2]**. Such devices require no fuel; only a temperature differential is needed to produce a finite power output. These devices, however, currently have low conversion efficiencies (6-8%) for power generation and have only found niche applications due to the high cost of supplying a large thermal input.

Recognizing that the principal trigger for power generation for TG devices is a heat gradient, two specific applications can be envisaged to have tremendous potential for the dismounted soldier. The first of these applications is a portable fuel-cell/TG hybrid system to rival batteries. For example, a portable microtubular SOFC system of 100 W by itself may not be competitive with batteries. However, it is anticipated that by recovering and utilizing the high-quality waste-heat generated by the fuel-cell system, the operation cost of the TG device is not expected only to decrease, but more importantly the efficiency of the fuel cell system would increase to allow for longer mission times without need for replacement. The second application takes further advantage of TGs to generate power derived from a natural heat source – the human body. The human body produces several tens of watts or more of heat energy depending if it is at rest or work **[3]**. By harnessing the natural heat energy from the body, it is conceivable that TGs, in the form of miniature modules that can be attached to the body or be incorporated into fabrics (so-called "*smart*" fabrics), could be used to drive low-power devices, such as sensors, thereby reducing the dependence on batteries.

1.2 Scope of Study

Despite the promising nature of fuel cells and thermoelectric generators as power sources, materials issues have hindered their practicality. Current state-of-the-art materials for fuel cell components are known to suffer long-term thermal degradation with unwanted chemical reactions occurring at the electrode-electrolyte interface. Mechanical failures also occur as a consequence of thermal expansion mismatches between the components resulting in physical cracks. Operating the stacks at lowered temperatures is expected to reduce these problems; however, this usually translates in poorer performance of current state-of-the-art materials and new materials must be found.

In the case of thermoelectric devices, the low efficiency of converting heat energy into electrical energy is directly linked to the difficulty of separating the highly interdependent Seebeck, electrical and thermal conductivity parameters in the materials that comprise such devices. A dimensionless parameter zT, called the figure-of-merit, which is used to gauge the performance of any thermoelectric material is defined by,

$$zT = \frac{S^2 \sigma T}{\kappa} \tag{1}$$

where S is the Seebeck coefficient, σ is the electrical conductivity, k is thermal conductivity and T is absolute temperature. Many of today's best bulk thermoelectric materials used commercially e.g. bismuth telluride have $zT \sim 1$. It is to be strongly noted that the majority of thermoelectrics are used for cooling applications, where the reverse phenomena, the Peltier effect is observed, i.e. supplying a voltage causes a cooling effect. For this reason, much effort has been undertaken to develop materials with $zT > 3$, where it is thought to be competitive with home refrigeration and beneficial for power generation applications **[4]**. In principle, there is no upper limit on zT and several theoretical studies have shown that it possible to achieve $zT > 3$ and more recently greater than 10 **[5]**. In practice, however, this goal has been elusive because of the interdependent nature of S, σ and k.

Given these challenges, the specific goals of this project were defined as follows: 1). to fabricate a non-anode supported solid oxide fuel cell architecture to mitigate durability problems associated with mechanical and chemical redox instabilities, 2). to develop novel cathode materials with superior physical properties than those offered by current state of the art materials, 3). to develop novel bulk thermoelectric transition-metal oxides with zT > 1 and, 4). to develop novel thermoelectric polymers for '*smart'* clothing.

This paper highlights the most significant results obtained for each of these tasks. The reader is referred to additional reports for further detailed technical descriptions of the work performed **[6-8].**

2 Porous Electrolyte-Supported Microtubular Solid Oxide Fuel Cell – Alberta Research Council

The core of any fuel cell system is the stack, which is comprised of an anode, cathode, and electrolyte. For SOFCs, these components are typically made from ceramic oxides, however, high temperature operation (> 900°C) can lead to durability issues. These include unwanted chemical reactions between cell components, mechanical cracks due to incompatible thermal expansion coefficients of the different cell components and degradation of the anode due to redox cycling. The detrimental effect of redox cycling at elevated temperatures can be seen Figure 1, which resulted in a decreased cell voltage from ~ 1.1 V to 0.57 V. In traditional cell designs, one component (the anode, cathode or electrolyte) is usually made thick enough to provide mechanical support for the other cell components. For example, as with an anode-supported single cell, the porous anode layer is made thicker relative to the cathode and electrolyte (several 100 μm or more). Being required to have > 98% theoretical density (for gas impermeability), it follows that the electrolyte component would make an ideal support. However, the practical limit to which the electrolyte layer can be made is limited by the high resistive losses if this layer is made to thick.

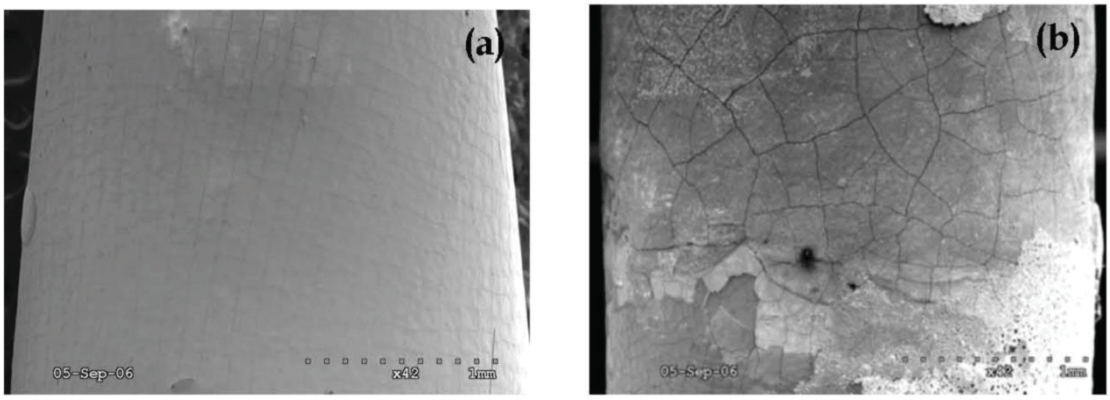

Figure 1: SEM micrographs of two different areas of the electrolyte layer showing extensive microcracking of redox cycled anode-supported single cell.

To circumvent this, a novel cell called the porous electrolyte support (PES) was designed and developed for this project. Specifically, a thick porous electrolyte support layer (~100μm) was deposited onto a very thin electrolyte layer, see Figure 2. By keeping the electrolyte layer thin (~10μm), resistive losses are kept to a minimum. An important feature of this design is that the thin gas-impermeable dense electrolyte layer and porous support structure are made of the same electrolyte material. Given the relatively high degree of porosity present in the support layer, the porous layer can be converted into either an anode or cathode by infiltrating the pores with the appropriate material, see Figure 3. This design also removes the sharp interface or material discontinuity between the electrolyte and electrode thereby reducing the problems associated with redox cycling and thermal expansion incompatibilities.

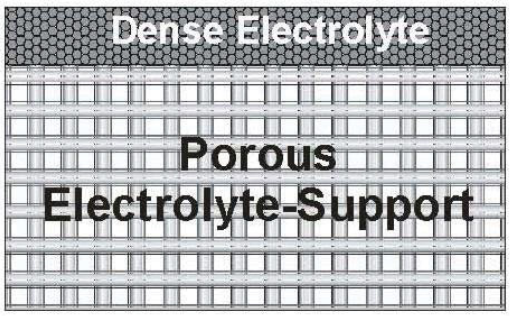

Figure 2: Illustration of a porous electrolyte supported partial single cell showing the dense electrolyte layer and the porous support layer.

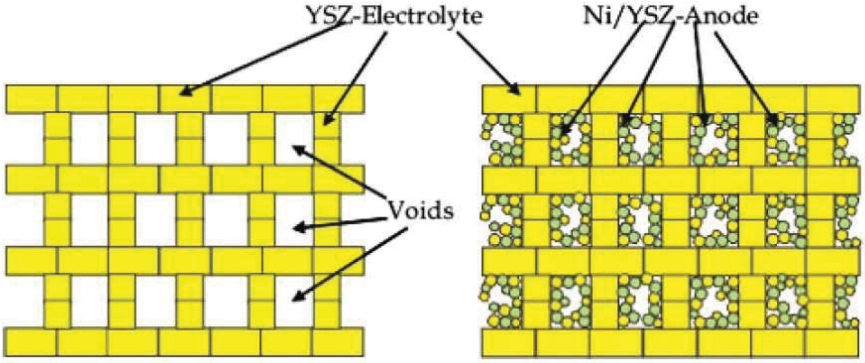

Figure 3: Illustration of a porous electrolyte support layer (a) before and (b) after infiltration of anode materials.

For this project, individual microtubular PES SOFCs (~ 10 cm long x 3-4 mm in diameter) were fabricated by electrophoretic deposition (EPD), see Figure 4. A variety of pore formers were tested to ensure pore formation in the support layer. Following this, complete single cells with anode and cathode were fabricated and electrochemically tested to determine the power generated from this design**.** The materials used in these cells are the traditional nickel-yttria-stabilized zirconia (Ni-YSZ) for the anode, lanthanum strontium manganite (LSM) for the cathode and yttria-stabilized zirconia (YSZ) for the electrolyte layers.

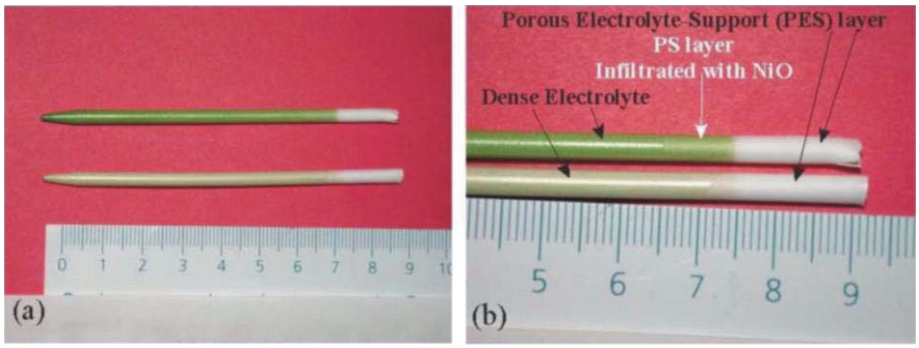

Figure 4: An example of two porous electrolyte-supported cells, the green sample was infiltrated with Ni phase before application of dense electrolyte layer.

Finally, a four-cell stack was built and subjected to long-term and thermal cycling tests to determine any significant degradation issues, the results of which are summarized below.

2.1 Long-term Testing of a Four-Cell PES Stack

The four-cell stack used for long-term testing was made by connecting four individual cells in series. Humidified hydrogen was used as the fuel at the anode with air as the oxidant on the cathode side. Prior to the start of long-term testing, the electrochemical stack performance was measured. A maximum power of ~427mW at 755^{o}C with an open circuit voltage (OCV) of ~ 4.37V (no power is drawn form the stack) was obtained, see Figure 5. This OCV value is close to the expected theoretical value, which demonstrates good gas sealing was maintained during the test. The stack was then allowed to operate for ~ 2200 hrs with a 200 mA current**.** The data collected, shown in Figure 6, shows three distinct regions labelled 'A', 'B' and 'C' with two anomalies shown. Region 'A' corresponds to data collected with a faulty temperature controller, while region 'C' corresponds to an interruption event with the data collection system. Despite these events, two major observations can be drawn from the data, the first of which is that the depletion of the hydrogen supply in region 'B' causes the cell voltage to drop precipitously to < 1.2 V. However, when the hydrogen was restored to the system, the stack voltage quickly recovered to its original value, which indicated no damage was done to the stack. This disruption in the hydrogen supply is the equivalent of undergoing one redox cycle, since during the disruption, air entered the anode side of the stack, which oxidized the Ni present in the anode to NiO. When the hydrogen supply resumed the NiO was reduced back to Ni with the stack operating voltage being recovered as before. Finally, the second important observation shows that at the end of 2183 hrs, the stack power was

determined to be 440mW at 755°C, which is slightly higher than the starting value of 427mW, which represents ~ 3% change in the stack operation during > 2000 hrs of operation.

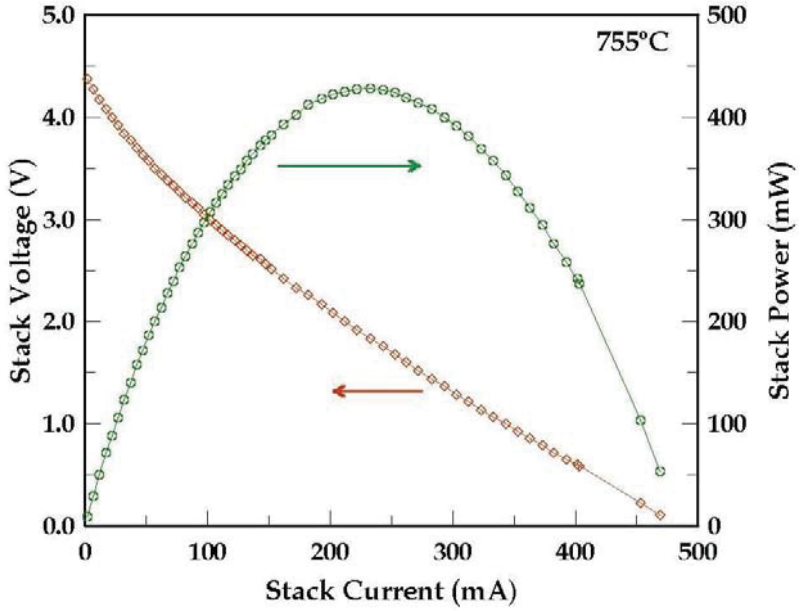

Figure 5: Electrochemical performance of the four cell short stack at 755°C before beginning of long term test.

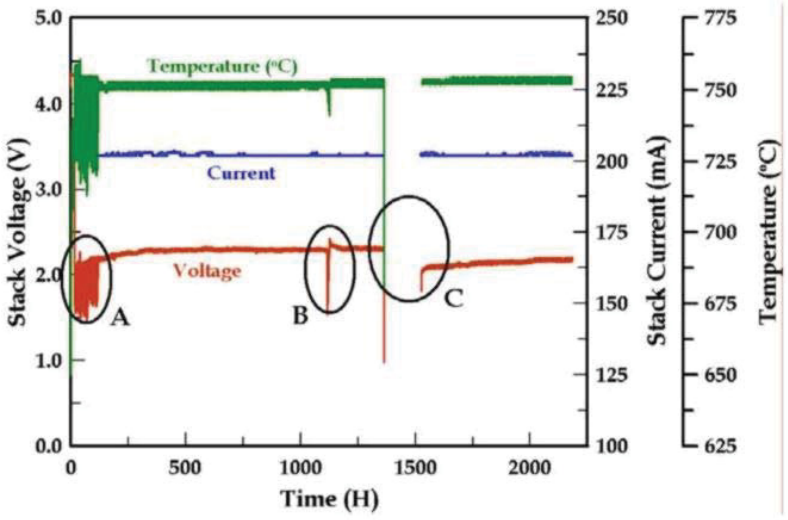

Figure 6: Long-term test of four-cell stack showing the stack operating voltage, temperature and current as a function of time at 755°.

2.2 Thermal Cycling

After completion of the long term test, the same four-cell stack was used for a thermal cycling test between 350°C and 710°C over a 500 hr period with 109 cycles. The OCV of the stack was relatively unchanged after the 109 thermal cycles, which strongly indicates that the stack remained intact and undamaged during the experiment, see Figure 7.

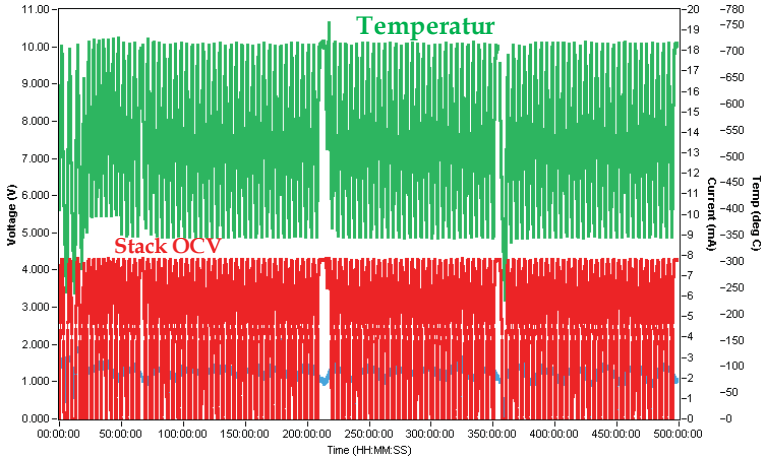

Figure 7: Thermal cycling test results of the four cell stack after long term g term test (109 cycles in total).

2.3 Conclusions

The results obtained from the four-cell PES stack attests to the robustness of the novel PES design when compared to conventional anode-supported cells. The new design reduces durability issues usually observed with traditional anode-supported cells by minimizing thermal expansion coefficient mismatches between the cell components and the effects of redox cycling. Consequently, this novel cell design shows promise for portable power applications where quick start-up times and multiple on/off operations are required. While these results are a step in the right direction to ensure increased durability and performance times, this work is in its early stages and, as such, has a low technology readiness level (TRL) of 2-3. To move this work forward, the following recommendations are made: 1). Further pore optimization studies to determine the optimum pore size distribution for electrode performance. 2). Development of new cathode materials to minimize polarization losses; state-of-the-art cathode materials can account for up to 65% polarization losses within a cell. 3). Prototype development targeting a 25W-100W portable system.

This page intentionally left blank

3 Ruddlesden-Popper Phases for SOFC Cathode Materials – DRDC-Atlantic

First generation SOFCs utilize yttria-stabilized zirconia (YSZ) as the electrolyte, which requires operation at high-temperatures (~1000 ^{o}C). Such high operating temperatures have severe implications for the long-term performance of the fuel-cell, which is closely associated with the type of cathode material used. In YSZ-based SOFCs, the cathode materials of choice are based on the mixed ionic-electronic conductors (MIECs) perovskites, $La_{1-x}Sr_xMnO_3$ (LSM). With continuous operation at high-temperatures, the cell components suffer unwanted chemical degradation, as evidenced by the formation of secondary phases at the cathode-electrolyte interface, such as the insulating $La_2Zr_2O_7$ and $SrZrO_3$. Furthermore, a mismatch in the thermal expansion coefficients (TECs) between the cathode and electrolyte results in cracking of the cell. As a consequence of these detrimental factors, there has been a push towards fuel cells that operate at an intermediate temperature range, which is broadly defined as being between 650^{o}-800^{o}C. Moving towards these lower temperatures, however, requires the discovery of new electrode materials, which retain the high electronic and ionic conductivity needed for physical transport processes. Furthermore, the performance of low-temperature SOFCs is highly dependent on cathode polarization losses, which can account for over 65% of the total loss and must be minimized to optimize the SOFC power densities

For this study, a series of novel materials based on the Ruddlesden-Popper crystallographic structure $A_{n+1}B_nO_{3n+1}$ (A = rare-earth, B = transition metal; *n = 3* where *n* is the number of perovskite layers), was investigated. When compared to the traditional perovskite materials, these materials have demonstrated increased oxygen mobility (as evidenced by high diffusion and surface exchange coefficients), relatively low thermal expansion coefficients, as well as the reasonably high electronic conductivity observed in the n = 1 phase $La_2NiO_{4+\delta}$ **[9-12].**

The crystal structure of the $La_2NiO_{4+\delta}$ phase is comprised of alternating perovskite ($LaNiO_3$) and rock-salt (LaO) layers, which allows for the accommodation of highly-labile excess oxygen-ions in the interstitial sites of the rock-salt layers. Consequently, a wide range of oxygen hyperstoichiometry, δ, is observed for $La_2NiO_{4+\delta}$ ($0 \leq \delta \leq 0.25$) **[13, 14].** Furthermore, it is known that the degree of hyperstoichiometry can be altered by varying the nature of the A and B cations **[15, 16].**

In this work, the following B-site doped series of compounds were prepared and characterized: $La_4Ni_{3-x}B_xO_{10-\delta}$ (A = Cu, Fe) and $La_{4-x}A_xNi_3O_{10-\delta}$ (A = Na, K and Sr). The results for the copper-doped system is presented, which has the most promise for cathode-use.

3.1 The $La_4Ni_{3-x}Cu_xO_{10-\delta}$ Solid-Solution

The Pechini method was used to prepare various compositions of the $La_4Ni_{3-x}Cu_xO_{10-\delta}$ solid-solution (x = 0.0, 0.1, 0.3 and 0.6). The products were generally black in colour, which were confirmed as being single-phase by X-ray powder diffraction. A typical pattern is shown in Figure 8. It was not possible to synthesize materials for x > 0.6, due to the instability of the crystal structure to accommodate larger amounts of the larger Cu^{2+} ions (relative to Ni^{2+}) on the B-site. Figure 9 shows the effect of increasing copper on the unit-cell volume; as more

copper is introduced the unit cell volume increases, which is consistent with the presence of Cu^{2+}. Furthermore, all compositions were confirmed to be oxygen deficient by potentiometric iodometric titration.

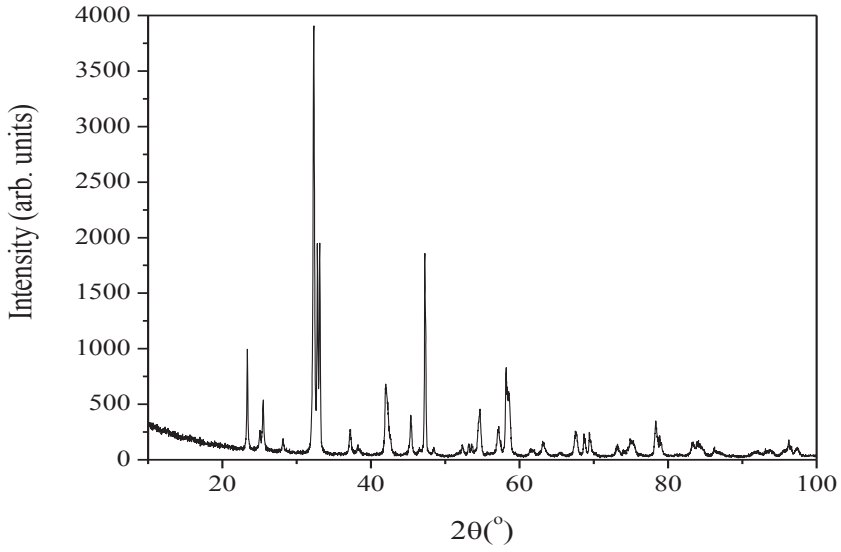

Figure 8: Typical XRD pattern for the $La_4Ni_{3-x}Cu_xO_{10-\delta}$ solid solution

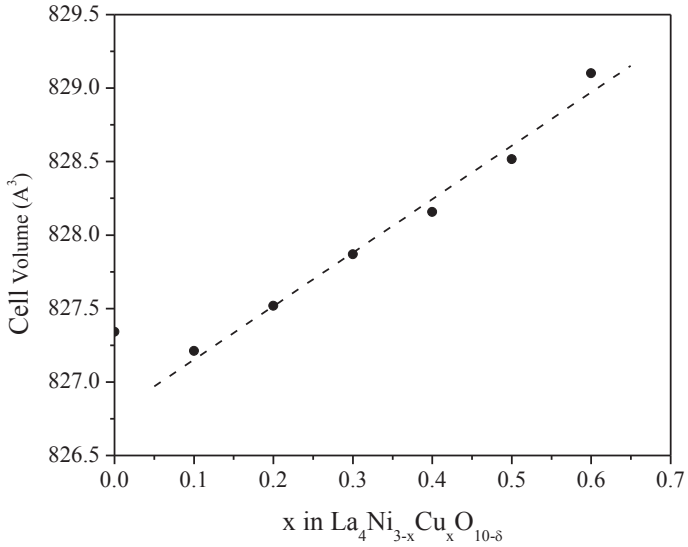

Figure 9: Unit cell volume vs copper content x.

The temperature dependence of the electrical conductivity measured by the van der Pauw method is shown in Figure 10. From this figure, it can be seen that increased copper doping results in an increase in the electrical conductivity with values for the x = 0.6 phase being significantly larger when compared to the state-of-the-art lanthanum strontium manganate, $La_{0.784}Sr_{0.196}MnO_3$, which was also characterized in-house. The electronic conduction mechanism of these materials are governed by $Ni(Cu)O_6$ octahedral units and the geometrical relationships of bond distances and bond angles as well as degree of band-filling influenced by the transition-metal ions. Clearly, there is a correlation with the increased unit cell volume observed previously and the enhanced conductivity observed.

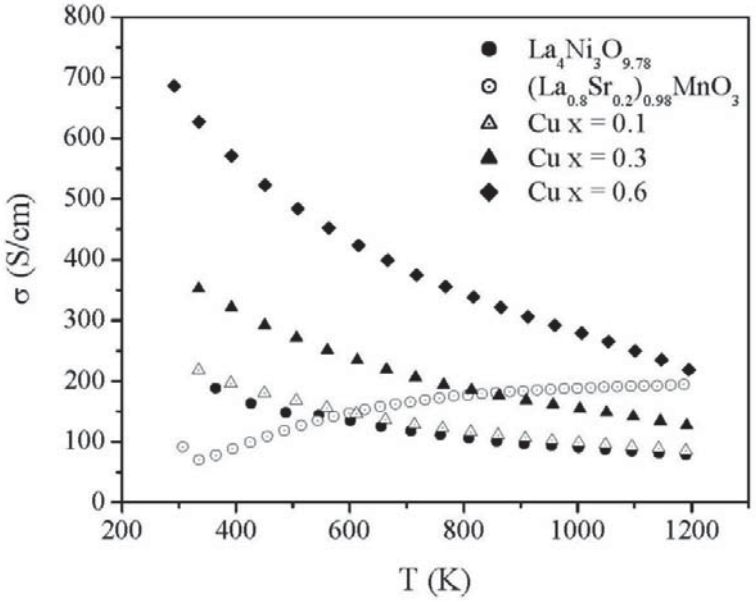

Figure 10: Electrical Conductivity of the $La_4Ni_{3-x}Cu_xO_{10-\delta}$ solid-solution (x = 0.0., 0.1, 0.3 and 0.6)

To determine the thermal expansion coefficients of the prepared materials, dilatometric data for the $La_4Ni_{3-x}Cu_xO_{10-\delta}$ phases in this study were collected from room temperature to 1173 K in air. The data is shown in Table 1, after correcting the data to take into account the thermal expansion of the sample stage. Interestingly, there is a very small, almost negligible, increase in α as x increases. The values obtained are within the acceptable 15% range when compared to the intermediate-temperature LSGM electrolyte ($\alpha \sim 12 \times 10^{-6}$ K^{-1}).

Table 1: Thermal Expansion Coefficients for the $La_4Ni_{3-x}Cu_xO_{10-\delta}$ solid-solution

x	TEC, α (10^{-6} K^{-1})
0.0	13.1
0.1	13.0
0.3	13.2
0.6	13.3

The normalized area-specific resistance for symmetrical cells was also determined with LSGM-9182 as the electrolyte, see Figure 11. From the data shown, the undoped, pure $La_4Ni_3O_{9.78}$ coated pellet has the lowest area-specific resistance; the presence of copper appears to worsen the electrode performance.

Finally, long-term stability determinations were carried out by preparing single pellets of pure material as well as pellets comprised of a 50:50 by weight of pure material mixed with electrolyte material, LSGM-9182. After firing in a furnace for two weeks at 1173K, x-ray powder diffraction confirmed no impurity phase formation.

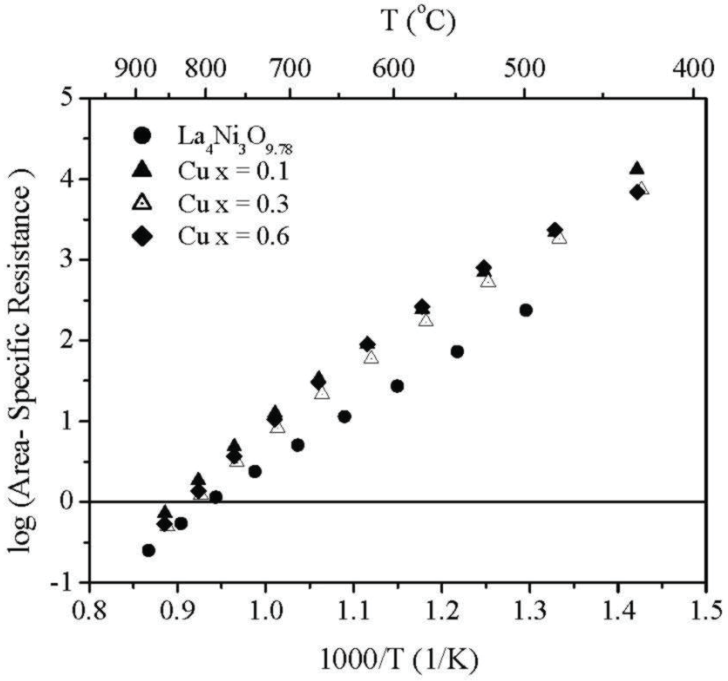

Figure 11: log (Area-specific Resistance) vs. 1000/T for $La_4Ni_3O_{9.78}$ and the Cu x = 0.1, 0.3 and 0.6 compositions in symmetrical cells with LSGM-9182 electrolyte.

3.2 Conclusions

The copper-doped higher-order RP phases, $La_4Ni_{3-x}Cu_xO_{10\pm\delta}$ (x = 0.0, 0.1, 0.3 and 0.6), were prepared and evaluated for their suitability as cathodes in intermediate temperature solid-oxide fuel cells. Characterizations of these materials reveal a significant increase of the electrical conductivity with copper content, as well as comparable and suitable thermal expansion coefficients with LSGM electrolyte. While gains have been made in these areas as well as long-term stability at high temperatures, more work is needed to optimize these properties as the area-specific resistance is still far below than what is required at the operating temperatures (log ASR ~ -0.15). These results underscore the challenges encountered in designing new materials in order to satisfy simultaneously the requirements for chemical and mechanical compatibility, long-

term stability, and superior physical properties (electrical conductivity and electrochemical performance). Recommendations for further work include further doping studies, for example rare-earth A-site doping or mixed A- and B-site doping, and electrochemical testing in full single cells with anode and electrolyte.

This page intentionally left blank

4 Thermoelectric Polymers for Smart Clothing – Université Laval

While the field of electronic conducting polymers is quite well-established, thermoelectric polymers are considered to be highly novel. This is largely due to the fact that the vast majority of thermoelectric materials research is centered upon inorganic materials such as skutterudites, half-Heusler alloys, clathrates, and pentatellurides. Organic-based materials afford certain advantages particularly for '*smart'* clothing due to the potential for flexibility and lower toxicity. Through simple modifications of the molecular structure, organic-based materials can be tuned for desired chemical and physical proprieties in a fairly large range.

To reiterate, the challenges in creating efficient thermoelectric materials is to achieve very good electronic conductors with poor thermal conductivity. Hence the main focus of this project is to improve zT by taking advantage of the inherent low thermal conductivity properties of polymers while maximising the electronic conductivity. For this study, two approaches were taken: 1). combining carbon nanotubes with polymers of high Seebeck values; carbon nanotubes are known to increase the electronic conductivity of polymers and, 2). synthesis of new poly (2,7 carbazole) derivatives. Unfortunately, very little success was obtained through combining carbon nanotubes with the targeted polymers; a consequence of not being able to fully functionalize all of the carbon nanotubes onto the polymer. The work and results from the latter approach is described below.

4.1 Novel poly(2,7 carbazole) derivatives [6, 17]

Three new poly (2,7 carbazole) derivatives were synthesized through a Suzuki coupling reaction, which are poly[N-9′-heptadecanyl-2,7-carbazole-alt-5,5-(2,2′-bithiophene)] (PCDT), poly[N-9′-heptadecanyl-2,7-carbazole-alt-5,5′-(2,2′-(1,4-phenylene)dithiophene)] (PCDTB) and poly[N-9′-heptadecanyl-2,7-carbazole-alt-5,5-(4′,7′-di-2-thienyl-2′,1′,3′-benzothiadiazole)] (PCDTBT) as shown in Figure 12.

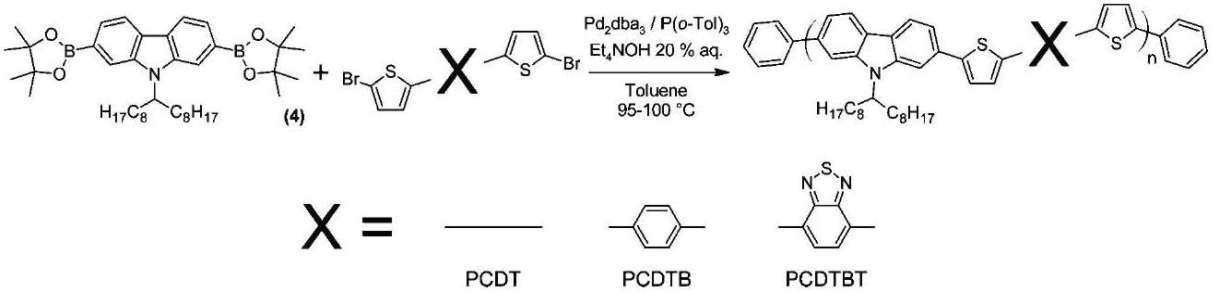

Figure 12: Synthesis of novel poly (2,7 carbazole) derivatives

The synthesized polymers had high molecular weights, good thermal stability as well as high glass transition temperatures, T_g, see Table 2 Furthermore, they were found to be soluble in common organic solvents such as tetrahydrofuran, chloroform, chlorobenznene, 1,2 dichlorobenzene and 1,2,4 trichlorobenzene. Solid-state UV-VIS spectra showed a bathochromic shift when compared to the solution spectra in trichlorobenzene at 135°C. Additionally, the absorption spectra of spin-coated PCDT and PCDTB thin films showed a vibronic splitting. Those two observations from the solution to the solid state spectrum comparison suggest higher structural organization in the solid state for both polymers, see Figure 13.

Table 2: Number-average molecular weight (M_n), polydispersity index (PDI), glass transition temperature (T_g), degradation temperature (T_d), electrochemical and optical properties of polycarbazole derivatives.

Polymer	M_n	PDI	T_g	T_m	ΔH	T_d	$E_{ox}^{onset\ a)}$	$E_{red}^{onset\ a)}$	E_g^{elec}	$E_g^{opt\ b)}$
	kDa		°C	°C	J.g^{-1}	°C	V vs SCE	V vs SCE	eV	eV
PCDT	25	1.7	90	230	0.97	450	0.76	-1.61	2.37	2.34
PCDTB	29	1.9	107	-	-	425	0.76	-1.69	2.45	2.41
PCDTBT	33	1.9	130	270	0.38	470	0.75	-1.10	1.85	1.88

[a]Measured with a cast film in a CH_3CN solution of 0.1M Bu_4NBF_4. SCE: standard calomel electrode; [b]Measurements performed on spin-coated films from the onset of the absorption band.

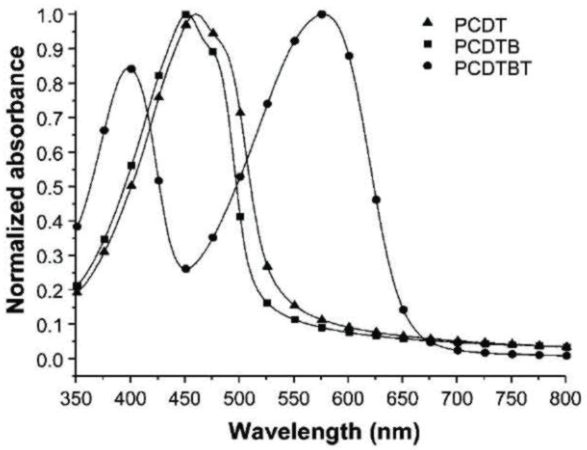

Figure 13: Solid-state UV-vis absorption spectra for PCDT, PCDTB, and PCDTBT.

Analyses from differential scanning calorimetry reveal one melting process for both the PCDT and PCDTBT at 230 and 270 °C, respectively; indicating the presence of some order in the solid state. Furthermore, X-ray diffraction (XRD) analyses on these polymer films support also this

assumption, see Figure 14. X-ray data suggest a lamellar packing for these polymers **[18, 19]**. For all polymers (PCDT, PCDTB and PCDTBT), the peak at ~4.5° corresponds to a layering distance, d = 19.6 Å, between sheets of each one of polymers chains, which pack in-plane perpendicular to their longitudinal axes **[18, 20].** The second broader peak at ~ 20.5° for PCDTBT and at ~19.5° for both of PCDTB and PCDT corresponds to a d spacing of ~4.4 Å and 4.6 Å, respectively. These represent the distance between the polymer chains within the layered planes **[18].** Typically, the relatively small d distance observed with PCDTBT might be related to favorable dipole-dipole and π-π interactions induced by the benzothiadiazole unit **[21, 22]**.

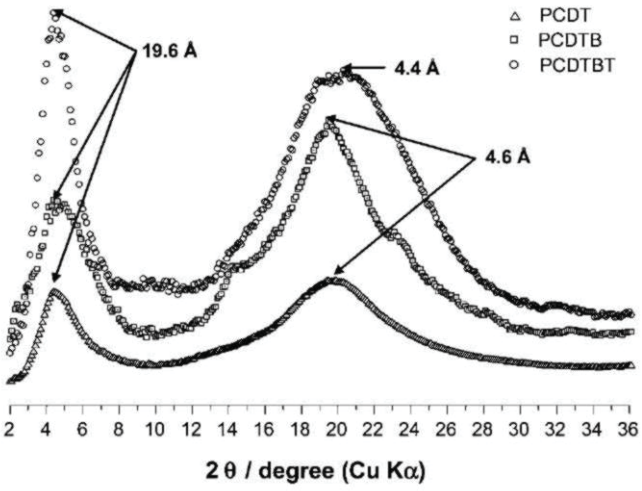

Figure 14: X-ray diffraction (XRD) graphs of PCDT, PCDTB, and PCDTBT films.

4.1.1. Electrical and thermoelectric properties of the polymers

Several studies have been already demonstrated that structural parameters can influence the charge transport properties and the electrical conductivity in conjugated polymers. For instance, orientation and solid state organization of the polymers may play a crucial role **[23, 24]**. Previously, it was shown through X-ray analyses that a structured state can be obtained by the introduction of secondary alkyl side chain on the carbazole unit and packing units such as benzene and benzothiadiazole moieties. These strong interchain interactions should facilitate the transport of the charge carriers through the polymeric structure **[25, 26]**. However, thermoelectric materials must combine both high electrical conductivities and high Seebeck coefficients. Unfortunately, the Seebeck coefficient usually decreases when the electrical conductivity is very high. As a typical example, Figure 15 shows the results obtained with PCDTBT films. With PCDTB and PCDT films, we noted lower values of thermoelectric parameters but similar behaviors. Figure 15 shows the experimental data of the Seebeck coefficient (S), electric conductivity (σ), and power factor (PF) obtained with PCDTBT for different doping levels with $FeCl_3$. In our calculations, it was assumed that all dopant molecules are $FeCl^{4-}$ species. The selection of $FeCl_3$ as a doping agent was guided by previous thermoelectric results obtained with other carbazole-based polymers **[27, 28]**. Positive values of the Seebeck coefficient S are obtained for all doped films,

indicating that the charge carriers are holes**[28]**. The best Seebeck coefficient (S ≈ 70 μV/K) was obtained with PCDTBT for low doping levels with $FeCl^{4-}$ species. PCDTBT films showed a Seebeck coefficient that was ~1 order of magnitude higher than that for polyaniline**[29]**.

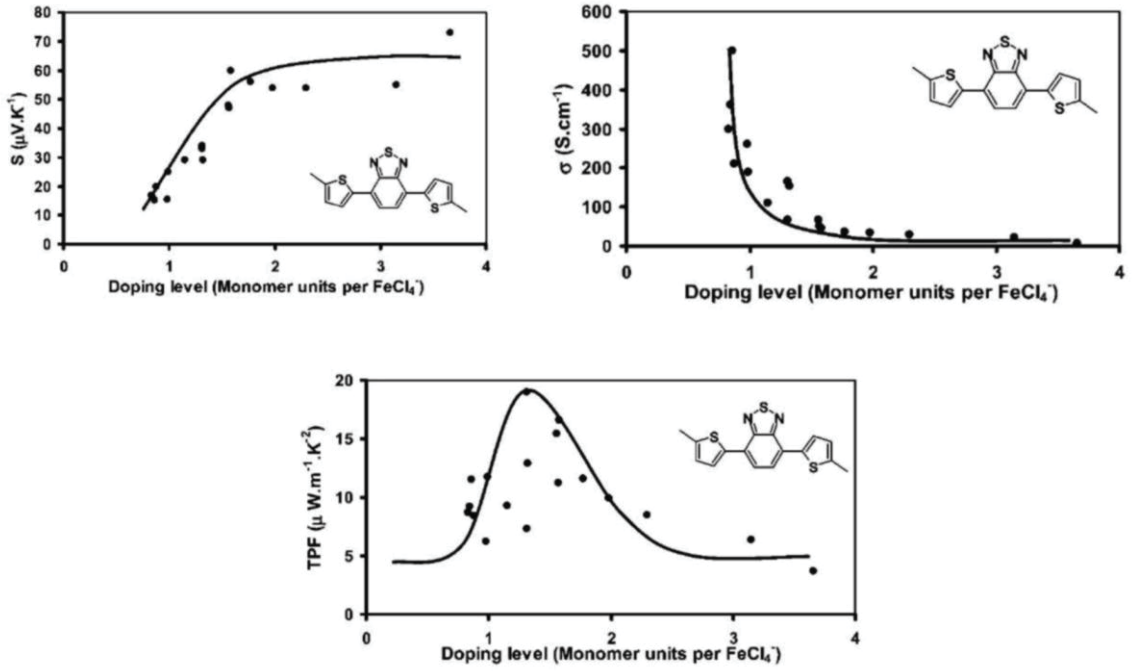

Figure 15: Seebeck coefficient, electrical conductivity, and power factor for FeCl3-doped PCDTBT films as a function of the doping level. Curves are drawn as guide lines for the eye.

The second parameter to be evaluated was the dependence of the electrical conductivity upon the doping level of PCDTBT films. The best electrical conductivity (500 S/cm) was obtained at high doping levels; this electrical conductivity is 2-3 times higher than that obtained with polyaniline, which is very similar to the best electrical conductivity that could be obtained with stretched poly(phenylene vinylene) derivatives**[30-32]**. Clearly, this electrical conductivity level is the highest among those reported for carbazole based polymers **[24, 27]**. Figure 15 also exhibits the doping dependence of the power factor. As the power factor is proportional to the square of the Seebeck coefficient, the high Seebeck coefficient of PCDTBT films resulted in a power factor that was ~40 times higher than that of polyaniline**[33]**. The best balance between the electrical conductivity and Seebeck coefficient led to a power factor of 19 mW m^{-1} K^{-2} for PCDTBT at intermediate doping levels. For comparison purposes, the maximum and optimized data of all these thermoelectric parameters obtained with PCDT, PCDTB, and PCDTBT films are summarized in Table 3. Polyaniline (PANI) films doped with (±)-10-camphorsulfonic acid (CSA), which is known to be a good thermoelectric polymer, was evaluated with our experimental setup and also was used for comparison**[34]**.

Table 3: Maximum conductivity, optimized conductivity (σ), maximum Seebeck coefficient, Seebeck coefficient (S), and thermoelectrical power factor (PF) of the PCDTBT, PCDTB, PCDT and PANI doped films.

	Maximum data		Optimized data		
	σ	S	σ	S	PF
	$S.cm^{-1}$	$\mu V.K^{-1}$	$S.cm^{-1}$	$\mu V.K^{-1}$	$\mu W.m^{-1}.K^{-2}$
PANI	160	6	160	5	0.4
PCDT	65	77	23	53	6.5
PCDTB	130	40	87	40	14
PCDTBT	500	70	160	34	19

4.1.2. Stability Studies of Thermoelectric Parameters

Among all parameters, the stability of the conducting polymers is an important issue for thermoelectric devices. Some polymers, such as iodine-doped polyacetylene, can show electric conductivities up to 60 000 S/cm **[35]** but limited stability (even in an inert environment). The stability of doped PCDTBT films (with $FeCl_3$) were tested while following their thermoelectric behaviour under different conditions. Figure 16 shows the thermoelectric parameters obtained as a function of time after doping in air (including a normal level of moisture). As it can be observed, after an initial decrease within the first few hours, the electrical conductivity of PCDTBT reaches a plateau at ~120 S/cm. This is partly due to its relatively low oxidation potential. In parallel, the Seebeck coefficient S shows a small increase, which ensures a relatively stable power factor of PF ≈ 17-18 μWm^{-1} K^{-2}.These data are among the best values reported up to now without physical treatment (annealing or stretching) **[30, 33]** and more importantly, it is the first time that good and relatively stable thermoelectric properties can be observed in this class of conjugated polymers. Based on these results, poly(2,7-carbazole) derivatives now seem to exhibit promising parameters for the future development of polymeric thermoelectric devices.

4.2 Conclusions

X-ray analyses have shown that a structured morphology can be obtained by introducing a secondary alkyl side chain on the carbazole unit and packing units such as benzene and benzothiadiazole unit along the conjugated backbone. Conductivity measurements indicate that, for identical processing parameters (the doped state), $FeCl_3$-doped PCDTBT films show the highest electrical conductivity with values up to 500 S/cm. Maximum conductivity values of conductivity reached 130 S/cm for PCDTB and 65 S/cm for PCDT, respectively. All these conductivity values are the highest reported for carbazole-based polymers. Moreover, the Seebeck coefficients are relatively high with values up to 70 μV/K. The best balance between these parameters led to power factor values of 19, 14, and 6.5 $\mu W\ m^{-1}\ K^{-2}$ for PCDTBT, PCDTB, and

PCDT, respectively. To the best of our knowledge, these data are among the highest thermoelectric parameters obtained with conjugated polymers that have been deposited without mechanical or thermal treatment. Moreover, these performances seem to be stable in air. To further increase the thermoelectric properties, it would be useful to evaluate the effects of some stretching or annealing as well as other *N*-containing conjugated polymers; it has been shown that this class of materials can lead to highly conducting materials.

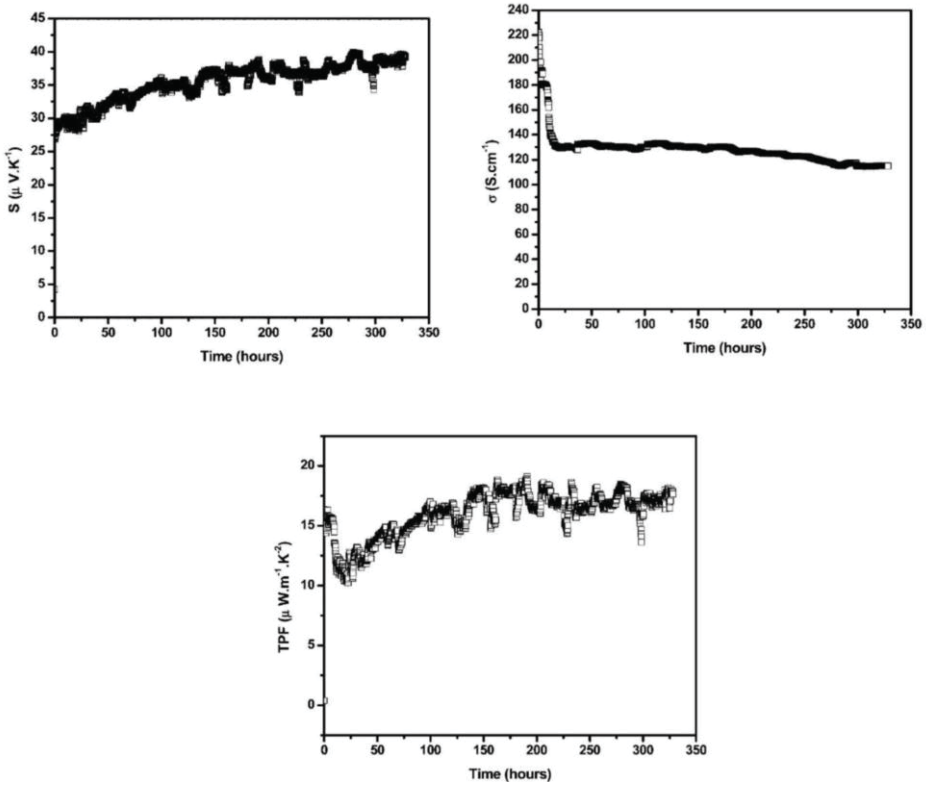

Figure 16: Stability study of thermoelectric parameters of doped PCDTBT

5 Development of Novel Transition Metal Oxide Thermoelectric Materials – University of Waterloo

Current state of the art bulk thermoelectric materials are based on bismuth telluride, Bi_2Te_3. In order to realize the hybridization of thermoelectric devices with high-temperature solid-oxide fuel cells (>600°C), it is necessary to have alternative materials to remove any toxicity problems associated with bismuth telluride (m.p. 580°C). To circumvent the toxicity problem, it was decided to investigate environmentally benign oxides. The most promising thermoelectric oxides are based on $Na_xCo_2O_4$ **[36, 37]** and other strongly correlated cobalt oxides **[38-40]**, however, cobalt is noted to be a toxic element as well. Encouraged by reports of strong performance of selected doped $SrTiO_3$ materials, with zT(850 K) = 0.2 for bulk $Sr_{0.9}La_{0.1}TiO_3$**[41]**, and zT(300 K) = 0.08 and zT(1073 K) = 0.27 for single crystals of $Sr_{1-x}La_xTiO_3$ **[42]**, this material was chosen as the parent material to be optimized via different doping and processing experiments. Previous work has also been reported on doping experiments with lanthanum or yttrium**[43]** on the A-site as well as niobium **[44]** on the B-site. In addition, the thermoelectric properties of perovskite-related Ruddlesden-Popper (RP) phases $SrO(SrTiO_3)_n$ (n = 1,2) doped with niobium and Ca-substituted $(Sr_{1-x}Ca_x)_3(Ti_{1-y}Nb_y)_2O_7$ (y = 0-0.2) were also investigated by others **[45, 46]**. In this study, five different material series were investigated, namely $SrTi_{1-x}Nb_xO_3$, $SrTi_{1-x}Ta_xO_3$, $SrTi_{1-x}Mo_xO_3$ and the double-substituted series, $Sr_{1-x}La_xTi_{1-x}Nb_xO_3$, and $Sr_{1-x}La_xTi_{1-x}Ta_xO_3$. The results for the double-substituted series are presented here.

5.1 Double-Substituted Transition Metal Oxides

A series of La, Ta double-substituted $Sr_{1-x}La_xTi_{1-x}Ta_xO_3$ with x= 0.01, 0.05 and 0.10, as well as a La, Nb double-substituted $Sr_{0.90}La_{0.10}Ti_{0.90}Nb_{0.10}O_3$ were investigated. These materials are all *n*-doped variants of the electron precise, insulating perovskite $SrTiO_3$. All materials were prepared by conventional solid state synthesis according to the scheme below:

$$(1-x)SrCO_3 + \frac{x}{2}La_2O_3 + (1-3x)TiO_2 + xTi_2O_3 + \frac{x}{2}Ta_2O_5 \rightarrow Sr_{1-x}La_xTi_{1-x}Ta_xO_3 + (1-x)CO_2$$

$$(1-x)SrCO_3 + \frac{x}{2}La_2O_3 + (1-3x)TiO_2 + xTi_2O_3 + \frac{x}{2}Nb_2O_5 \rightarrow Sr_{1-x}La_xTi_{1-x}Nb_xO_3 + (1-x)CO_2$$

Single phase determinations were done by Rietveld refinements of x-ray data with impurity reflections present, see Figure 17. Table 4 compares the lattice parameters, residual values, and U values of the Rietveld refinements. All these doping experiments led to an increase in the unit cell size, e.g. from a = 3.901 Å for $SrTiO_3$ to 3.905 Å for $Sr_{0.99}La_{0.01}Ti_{0.99}Ta_{0.01}O_3$ and 3.915 Å for $Sr_{0.90}La_{0.10}Ti_{0.90}Ta_{0.10}O_3$. All R_P values are below 5%, indicating successful refinements and thus homogenous doping. The phase purity can further be testified by the comparable refinement results with $SrTi_{0.90}Ta_{0.10}O_3$, since the Electron Microprobe Analysis of $SrTi_{0.90}Ta_{0.10}O_3$, confirmed its homogeneity as well as the Ti/ Ta ratio with the analysis result being $Sr_{1.00(1)}Ti_{0.89(2)}Ta_{0.10(2)}O_{2.99(2)}$ **[47],** see Figure 18. It was not possible to refine reliably the occupancy of doped elements, and the isotropic thermal displacement parameters of oxygen (U_O). Therefore the occupancies were fixed to equal the nominal composition, and U_O fixed at 0.02 Å^2. The refined isotropic thermal displacement parameters may be used to justify this approach.

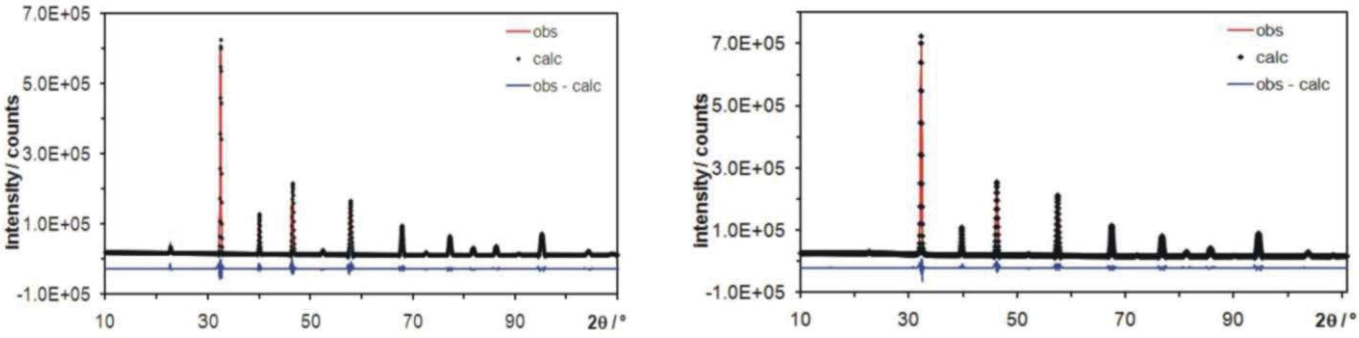

Figure 17: Rietveld refinements on $SrTiO_3$ (left) and $Sr_{0.9}La_{0.1}Ti_{0.9}Ta_{0.1}O_3$ (right).

Table 4: Rietveld refinements on pure and n*-type doped $SrTiO_3$, space group $Pm\bar{3}m$. U_O was fixed to be 0.02 Å^2 in all cases.*

Composition	*a*/Å	R_{F2}/%	R_P/%	wR_P/%	U_{Sr}/Å^2	U_{Ti}/Å^2
$SrTiO_3$	3.9008(2)	2.81	4.19	6.31	0.0170(6)	0.0203(6)
$SrTi_{0.90}Ta_{0.10}O_3$	3.9145(2)	3.00	3.52	4.16	0.0127(5)	0.0213(5)
$Sr_{0.90}La_{0.10}Ti_{0.90}Nb_{0.10}O_3$	3.9132(2)	3.04	3.04	4.59	0.0181(5)	0.0159(5)
$Sr_{0.99}La_{0.01}Ti_{0.99}Ta_{0.01}O_3$	3.9051(1)	2.77	3.82	5.30	0.0177(5)	0.0193(5)
$Sr_{0.95}La_{0.05}Ti_{0.95}Ta_{0.05}O_3$	3.9111(2)	2.30	3.36	4.27	0.0166(5)	0.0189(6)
$Sr_{0.90}La_{0.10}Ti_{0.90}Ta_{0.10}O_3$	3.9150(2)	3.89	3.25	5.11	0.0209(7)	0.0181(6)

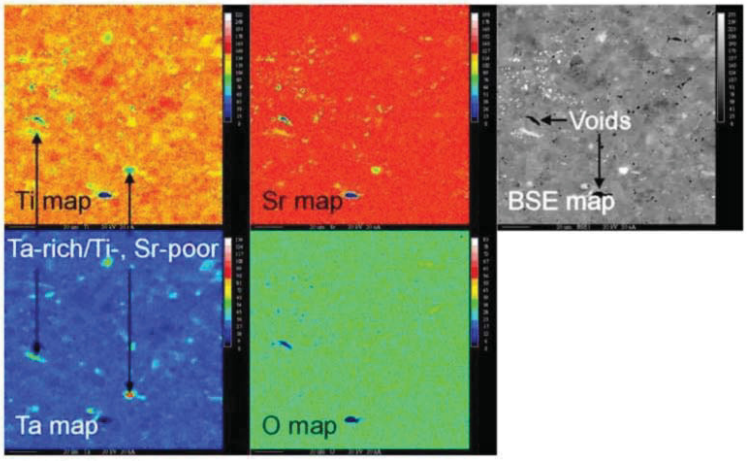

Figure 18: Electron probe microanalysis maps of $SrTi_{0.90}Ta_{0.10}O_3$.

Electronic structure calculations were carried out for pure $SrTiO_3$ and $Sr_{0.875}La_{0.125}Ti_{0.875}Ta_{0.125}O_3$. Since both La and Ta atoms provide one more valence electron per atom than the replaced Sr and Ti atoms, a doping level of x = 0.125 formally corresponds to 4.2×10^{21} electrons per cm^3, which is at the upper border of the ideal carrier concentration for thermoelectrics. Therefore, the samples investigated cover the large (formal) carrier concentration range between 3.4×10^{20} ($Sr_{0.99}La_{0.01}Ti_{0.99}Ta_{0.01}O_3$) and 3.4×10^{21} ($Sr_{0.90}La_{0.10}Ti_{0.90}Ta_{0.10}O_3$) electrons per cm^3.

The rather large computed gap of $SrTiO_3$ of 1.30 eV (Figure 19) indicates that the ideal operating temperature for thermoelectrics based on variants of this material will be high. **[48]** Its faint yellow color implies that the actual band gap is even larger, noting that the size of the gap is usually underestimated in density functional theory (DFT) calculations. The band structure of the model $Sr_{0.875}La_{0.125}Ti_{0.875}Ta_{0.125}O_3$ exhibits a gap of 1.4 eV but the Fermi level falls into a region of steep bands within the conduction band.

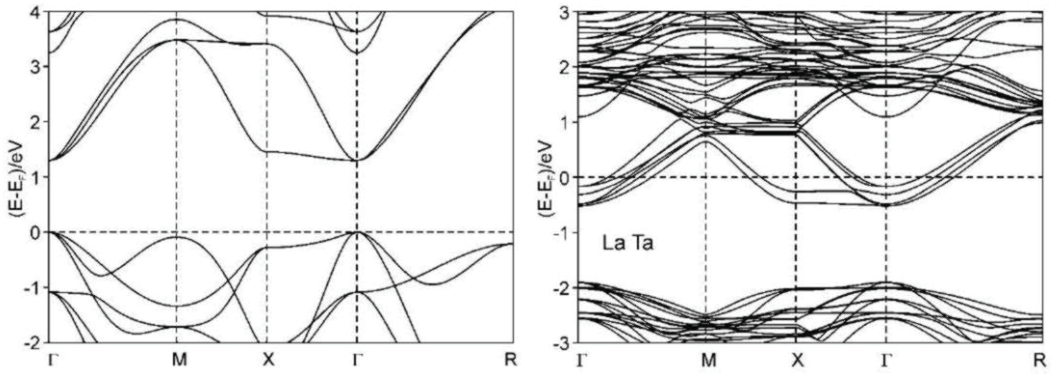

Figure 19: Band structures of $SrTiO_3$ (left), and $Sr_7LaTi_7TaO_{24}$ (right)

A very flat band occurs directly above the gap of $SrTiO_3$, and runs almost horizontally along *a** (Γ -> X), indicative of a high effective mass, *m**, and thus a large Seebeck coefficient of

appropriately *n*-doped $SrTiO_3$. The degeneracy at the Γ point also indicates a high Seebeck coefficient (equation 2) **[49]**. On the other hand, highly disperse bands run along Γ → M and Γ → R, which points towards high mobility, μ, and thus high electrical conductivity (equation 3) **[50-52]**.

$$S = \frac{8\pi^2 k_B^2}{3eh^2} m^* T \left(\frac{\pi}{3n} \right)^{2/3} \tag{2}$$

$$\sigma = ne\mu \tag{3}$$

with k_B = Boltzmann constant, e = electron charge, h = Planck constant, n = charge carrier concentration. The band structure of $Sr_{0.875}La_{0.125}Ti_{0.875}Ta_{0.125}O_3$ is very comparable but the degeneracies are in part destroyed as a consequence of the lower symmetry. Depending on the exact doping level, the Fermi level will be lower, possibly falling into the region with the flat bands just above the gap.

In all four samples compacted via spark plasma sintering (SPS), the absolute Seebeck values increase smoothly with increasing temperature, see Figure 20. For the La- and Ta-doped samples, the absolute Seebeck values decrease with increasing doping level (from -150 μVK^{-1} for x = 0.01 to -50 μVK^{-1} for x = 0.10 at 320 K), which is comparable to the results of Ta only doped samples **[47]**. The La- and Nb-doped sample has a higher absolute Seebeck value compared to the corresponding La- and Ta-doped sample, $Sr_{0.90}La_{0.10}Ti_{0.90}Ta_{0.10}O_3$ (-75 μVK^{-1} vs. -50 μVK^{-1} at 320K). The hot-pressed samples follow the same trends, with slightly higher values that range from -270 μVK^{-1} to -75 μVK^{-1} at 320 K, see Figure 21.

The electrical conductivity increases rapidly with increasing temperature for the samples with x = 0.05 and x = 0.10 over the whole temperature range measured, which is indicative for dominantly temperature-activated conduction. The Nb material exhibits higher electrical conductivity, compared to the analogous Ta material, which may be due to its higher density. On the other hand, the electrical conductivity for the lowest doped sample (x = 0.01) is higher than for the highly doped samples in the measured temperature range and is decreasing with increasing temperature, indicative of a significant number of extrinsic charge carriers.

The above is true for both SPS and hot-pressed samples with x = 0.01, with the hot-pressed sample having lower absolute values, e.g. at room temperature 65 $\Omega^{-1}cm^{-1}$, compared to 600 $\Omega^{-1}cm^{-1}$ for the SPS sample. The latter is likely in part a consequence of the higher density of the SPS sample of 5.1 gcm^{-3} vs. 4.8 gcm^{-3}, i.e. 99% vs. 93% of the theoretical maximum. This higher density is likely a consequence of the higher pressure and temperature involved as well as localized heating, occurring with smaller grain boundary effects. Small differences in the charge carrier concentration, however, cannot be excluded because different samples - albeit of the same nominal composition - were used.

The thermal conductivity, κ, increases with the increase of x, and $Sr_{0.90}La_{0.10}Ti_{0.90}Nb_{0.10}O_3$ exhibits a higher thermal conductivity compared to $Sr_{0.90}La_{0.10}Ti_{0.90}Ta_{0.10}O_3$. The absolute values are lower than the numbers from Muta et al.**[41]** for $Sr_{0.9}La_{0.1}TiO_3$, with κ (300 K) = 6.8 $Wm^{-1}K^{-1}$ except for $Sr_{0.99}La_{0.01}Ti_{0.99}Ta_{0.01}O_3$. The hot-pressed samples exhibit the same trends as the SPS

samples, albeit with lower values, which supports the above-mentioned larger grain boundaries of the hot-pressed samples.

Like in the other cases of doped $SrTiO_3$, *zT* increases with increasing temperature (Figure 20). For the hot-pressed sample, *zT* values could not be obtained because of the different temperature ranges of Seebeck, electrical conductivity and thermal conductivity measurements. The lowest doped sample, $Sr_{0.99}La_{0.01}Ti_{0.99}Ta_{0.01}O_3$, exhibits the largest zT, e.g. 0.13 at 660 K, comparable with $SrTi_{0.95}Ta_{0.05}O_3$ (0.10 at 650 K) **[47]**, while the zT values of the other double substituted samples remain under 0.003. It is postulated that zT will continue to increase at higher temperatures, and ongoing investigations are planned to reveal the extent of that expected increase. Moreover, as $Sr_{0.90}La_{0.10}Ti_{0.90}Nb_{0.10}O_3$ has higher zT values than $Sr_{0.90}La_{0.10}Ti_{i0.90}Ta_{0.10}O_3$ over the whole temperature range, an investigation of more, differently doped Nb materials appears to be promising.

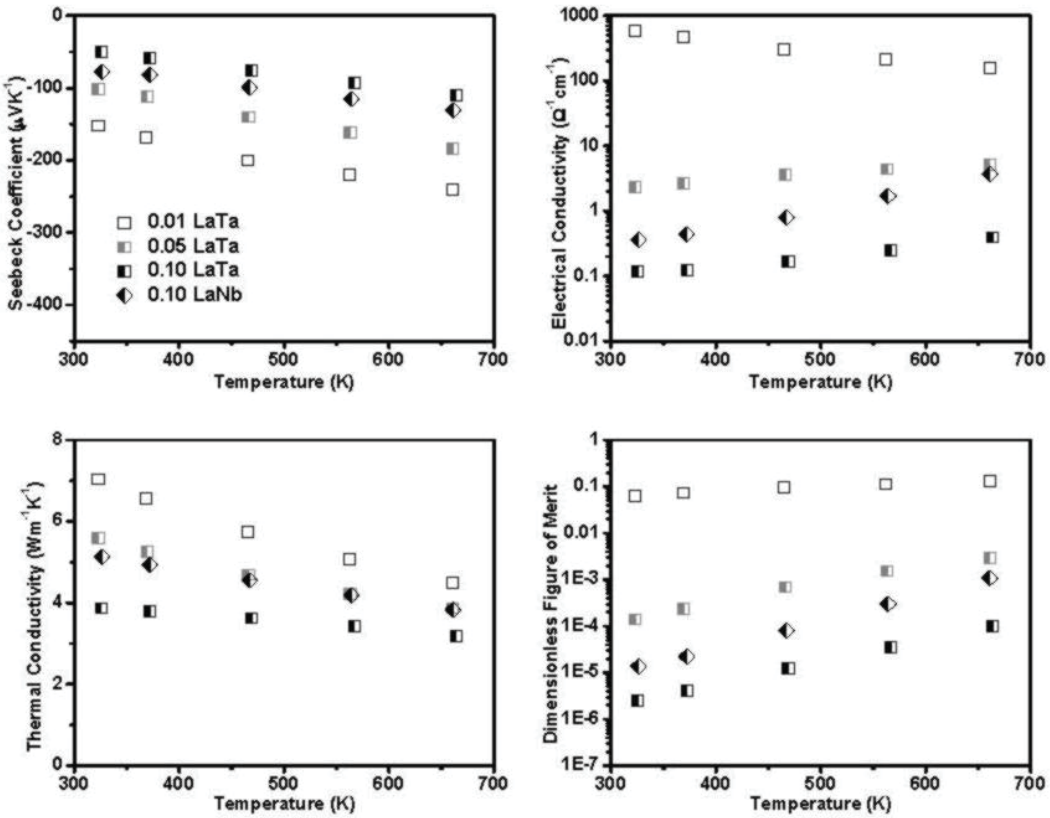

Figure 20: Thermoelectric properties of $Sr_{1-x}La_xTi_{1-x}Nb_xO_3$ and $Sr_{1-x}La_xTi_{1-x}Ta_xO_3$ (compacted via SPS).

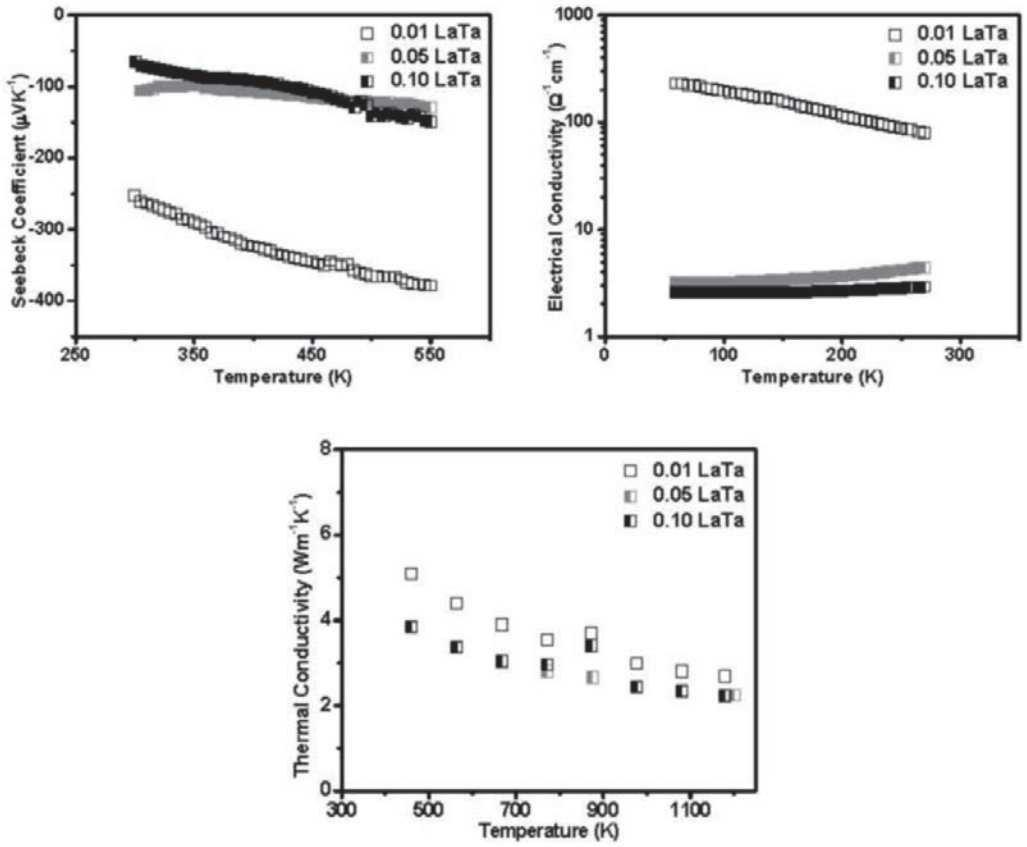

Figure 21: Thermoelectric properties of $Sr_{1-x}La_xTi_{1-x}Nb_xO_3$ and $Sr_{1-x}La_xTi_{1-x}Ta_xO_3$ (compacted via hot-pressing). zT values could not be obtained because of the different temperature ranges of the respective property measurements.

5.2 Conclusion

The investigated materials comply with all of the initial criteria of low cost, low toxicity and high thermal stability. The doping experiments carried out here were successful as they led to significant improvements of the thermoelectric properties of the parent material $SrTiO_3$. Figure of merit, *zT*, values were achieved in excess of 0.13 for x = 0.01 in $Sr_{1-x}La_xTi_{1-x}Ta_xO_3$; higher *zT* values are likely to occur at higher temperatures. Still, however, the zT values are too low for practical use of these materials in thermoelectric devices. It is suggested that additional doping experiments with intermediate x, e.g. x = 0.02 and 0.04, be carried out in the future to identify the best charge carrier concentration, in particular using Nb instead of Ta. Moreover, as the higher density samples appear to perform better, close attention needs to be paid to optimizing the pressing procedure. Further optimization will be required in order to become competitive with, for example, the more toxic *p*-type Na_xCoO_2.

6 Concluding Remarks

The work described in this report highlights the most important results to come out of the TIF project, "Advanced Materials for Soldier Power Applications through Waste Heat Recovery". While the operation principles of fuel cells and thermoelectric generators have been known since the 1800's, materials issues have plagued their commercial success. In the case of fuel cells, durability and fuel supply issues are challenges while for thermoelectric generators, very low conversion efficiencies is the norm. The goal of this project sought to make significant advancements in the desired materials properties to pave the way for the future hybridization of these two technologies. Such advancements would lead to benefits for the dismounted soldier by enabling these technologies to reduce the logistics burden of size and weight while providing high energy conversion efficiencies. While limited successes have been gained in this project, specifically, the improved SOFC microtubular porous electrolyte support architecture and improved thermoelectric polymers, much work is still required for materials development to achieve high power densities and performance longevity for fuel cells and high figure of merits >1 for thermoelectric devices.

Despite these challenges, the defence potential for these two technologies is evident and remains promising. Today, commercial portable fuel cells (25W-100W) exist on the market such as those based on hydrogen (e.g. Smart Fuel Cells), reformed methanol (e.g. Ultracell) and propane (Adaptvie Materials Inc.). These units, however, are at technology readiness levels of 6-7, as issues for fuel resupply and performance-related (materials) issues remain to be resolved. The technology readiness level for thermoelectric devices, particularly '*smart'* clothing, is even lower. However, recent significant advances have been made with thin-film fabrication methods, which have produced zT values of ~ 2-3. With this in mind the following recommendations are made: a). provide support to the Alberta Research Council to mature stack design for device prototype, b). continue development of novel materials for solid oxide materials and c). continue materials development of thermoelectric oxides and polymers. The high-risk associated with these activities limit the funding avenues for immediate follow-on plans in these areas. As a result of this work, core competencies were developed in fuel cells and thermoelectrics, as well as microcogeneration (simultaneous production of heat and power). Follow-on activities in the latter include the evaluation of a 25W SOFC portable unit and a 1 kW microcogeneration PEMFC system, which are currently underway.

This page intentionally left blank

7 References

[1] Sarkar, P., Rho, H., Yamarte, L. and Johnson, L. Sixth European Solid Oxide Fuel Cell Forum Proceedings. In *European Fuel Cell Forum 2004*. Lucerne, Switzerland.

[2] MacDonald, D. (1962). *Thermoelectricity: An Introduction to the Principles*, New York: Wiley.

[3] Clark, R. P. and Edholm, O. G. (1985). *"Man and His Thermal Environment*, London: Edward Arnold Publishers Ltd.

[4] Nolas, G. S., Sharp, J. and Goldsmid, H.J. (2001). *Thermoelectrics: Basic Principles and New Materials Developments*. Springer Series in Materials Science ed. Hull and R., O., R.M., Sakaki, H. and Zunger, A. Vol. 45, Germany: Springer-Verlag.

[5] Humphrey, T. E. and Linke, H. (2005). *Phys. Rev. Lett.*, 94, 096601-1 to 096601-3.

[6] LeClerc, M. Thermoelectric Polymers for Smart Clothing. (CR2009-076). DRDC Atlantic.

[7] Kleinke, H. Development of Novel Transition Metal Oxide Thermoelectric Materials. (CR2009-175).

[8] Yamarte, L. and Sarkar, P. (2009). Development and Fabrication of a Novel Non Anode-Supported Microtubular Fuel Cell. (CR2009-138). Alberta Research Council.

[9] Kilner, J. A. and Shaw, C. K. M. (2002). Mass transport in La2Ni1-xCoxO4 +[delta] oxides with the K2NiF4 structure. *Solid State Ionics*, 154-155, 523.

[10] Kharton, V. V., Viskup, A.P., Naumovich, E.N. and Marques, F.M.B. (1999). Oxygen ion transport in La2NiO4-based ceramics. *J. Mater. Chem.*, 9 (10), 2623-2629.

[11] Skinner, S. J. and Kilner, J. A. (2000). Oxygen diffusion and surface exchange in La2-xSrxNiO4+[delta]. *Solid State Ionics*, 135 (1-4), 709.

[12] Shaw, C. K. M. and Kilner, J. A. (2000). Investigation of oxygen transport properties in La2Ni1-xCoxO4+d for ITSOFC cathodes. In *Fourth European Solid Oxide Fuel Cell Forum*. 2000. Lucerne, Switzerland.

[13] Rice, D. E. and Buttrey, D. J. (1993). An X-Ray Diffraction Study of the Oxygen Content Phase Diagram of La2NiO4+d. *Journal of Solid State Chemistry*, 105 (1), 197.

[14] Jorgensen, J. D., Dabrowski, B., Pei, S., Richards, D. R. and Hinks, D. G. (1989). Structure of the interstitial oxygen defect in La2NiO4+d. *Phys. Rev. B*, 40 (4), 2187-2199.

[15] Boehm, E., Bassat, J.M., Mauvy, F., Dordor, P., Grenier, J.C. and Pouchard, M. (2000). Thermal Stability and Mixed conducitivty in Ln2Ni1-xCuO4+d (Ln=La, Pr, Nd) for SOFC cathodes. In *Fourth European Solid Oxide Fuel Cell Forum*. 2000. Lucerne, SwizTerland.

[16] Bassat, J. M., Boehm, E., Grenier, J.C., Mauvy, F., Dordor and Pouchard, M. (2002). YSZ-Supported cathodes of rare-earth nickelates Ln2NiO4+d for ITSOFC (650C). In *Fifth European Solid Oxide Fuel Cell Forum*. 2002. Lucerne, Switzerland.

[17] Aich, R. B., Blouin, N., Bouchard, A. and Leclerc, M. (2009). Electrical and Thermoelectric Properties of Poly(2,7-Carbazole) Derivatives. *Chemistry of Materials*, 21 (4), 751-757.

[18] Kinder, L., Kanicki, J. and Petroff, P. (2004). Structural ordering and enhanced carrier mobility in organic polymer thin film transistors. *Synthetic Metals*, 146 (2), 181-185.

[19] Lim, E., Jung, B.-J., Lee, J., Shim, H.-K., Lee, J.-I., Yang, Y. S.and Do, L.-M. (2005). Thin-Film Morphologies and Solution-Processable Field-Effect Transistor Behavior of a Fluoreneâˆ’Thieno[3,2-b]thiophene-Based Conjugated Copolymer. *Macromolecules*, 38 (10), 4531-4535.

[20] Blouin, N., Michaud, A., Gendron, D., Wakim, S., Blair, E., Neagu-Plesu, R., Belletete, M., Durocher, G., Tao, Y. and Leclerc, M. (2007). Toward a Rational Design of Poly(2,7-Carbazole) Derivatives for Solar Cells. *Journal of the American Chemical Society*, 130 (2), 732-742.

[21] Chen, C.-T. (2004). Evolution of Red Organic Light-Emitting Diodes: Materials and Devices. *Chemistry of Materials*, 16 (23), 4389-4400.

[22] Yamamoto, T., Arai, M., Kokubo, H. and Sasaki, S. (2003). Copolymers of Thiophene and Thiazole. Regioregulation in Synthesis, Stacking Structure, and Optical Properties. *Macromolecules*, 36 (21), 7986-7993.

[23] Wakim, S., Blouin, N., Gingras, E.,Tao, Y.,Leclerc, M. (2007). Poly(2,7-carbazole) Derivatives as Semiconductors for Organic Thin-Film Transistors. *Macromolecular Rapid Communications*, 28 (17), 1798-1803.

[24] Donley, C. L., Zaumseil, J., Andreasen, J. W., Nielsen, M. M., Sirringhaus, H., Friend, R. H. and Kim, J.-S. (2005). Effects of Packing Structure on the Optoelectronic and Charge Transport Properties in Poly(9,9-di-n-octylfluorene-alt-benzothiadiazole). *Journal of the American Chemical Society*, 127 (37), 12890-12899.

[25] Letizia, J. A., Salata, M. R., Tribout, C. M., Facchetti, A., Ratner, M. A. and Marks, T. J. (2008). n-Channel Polymers by Design: Optimizing the Interplay of Solubilizing Substituents, Crystal Packing, and Field-Effect Transistor Characteristics in Polymeric Bithiophene-Imide Semiconductors. *Journal of the American Chemical Society*, 130 (30), 9679-9694.

[26] Kline, R. J., DeLongchamp, D. M., Fischer, D. A., Lin, E. K., Richter, L. J., Chabinyc, M. L., Toney, M. F., Heeney, M. and McCulloch, I. (2007). Critical Role of Side-Chain Attachment Density on the Order and Device Performance of Polythiophenes. *Macromolecules*, 40 (22), 7960-7965.

[27] Levesque, I., Bertrand, P.-O., Blouin, N., Leclerc, M., Zecchin, S., Zotti, G., Ratcliffe, C. I., Klug, D. D., Gao, X., Gao, F. and Tse, J. S. (2007). Synthesis and Thermoelectric Properties of Polycarbazole, Polyindolocarbazole, and Polydiindolocarbazole Derivatives. *Chemistry of Materials*, 19 (8), 2128-2138.

[28] Lévesque, I., Gao, X., Klug, D. D., Tse, J. S., Ratcliffe, C. I. and Leclerc, M. (2005). Highly soluble poly(2,7-carbazolenevinylene) for thermoelectrical applications: From theory to experiment. *Reactive and Functional Polymers*, 65 (1-2), 23-36.

[29] Yakuphanoglu, F. and Senkal, B. F. (2007). Electronic and Thermoelectric Properties of Polyaniline Organic Semiconductor and Electrical Characterization of Al/PANI MIS Diode. *The Journal of Physical Chemistry C*, 111 (4), 1840-1846.

[30] Hiroshige, Y., Ookawa, M. and Toshima, N. (2007). Thermoelectric figure-of-merit of iodine-doped copolymer of phenylenevinylene with dialkoxyphenylenevinylene. *Synthetic Metals*, 157 (10-12), 467-474.

[31] Jacobo, S. E., Aphesteguy, J. C., Lopez Anton, R., Schegoleva, N. N. and Kurlyandskaya, G. V. (2007). Influence of the preparation procedure on the properties of polyaniline based magnetic composites. *European Polymer Journal*, 43 (4), 1333-1346.

[32] Hiroshige, Y., Ookawa, M.and Toshima, N. (2006). High thermoelectric performance of poly(2,5-dimethoxyphenylenevinylene) and its derivatives. *Synthetic Metals*, 156 (21-24), 1341-1347.

[33] Toshima, N. (2002). Conductive polymers as a new type of thermoelectric material. *Macromolecular Symposia*, 186 (1), 81-86.

[34] Cao, Y., Qiu, J. and Smith, P. (1995). Effect of solvents and co-solvents on the processibility of polyaniline: I. solubility and conductivity studies. *Synthetic Metals*, 69 (1-3), 187-190.

[35] Zhan, X., Xu, S., Yang, M., Shen, Y. and Wan, M. (2002). Vibration and X-ray photoelectron spectroscopies of FeCl3-doped poly(p-diethynylbenzene). *European Polymer Journal*, 38 (10), 2057-2061.

[36] Terasaki, I. (2003). Transport properties and electronic states of the thermoelectric oxide NaCo2O4. *Physica B*, 328 (1-2), 63-67.

[37] Wang, Y., Rogado, N. S., Cava, R. J. and Ong, N. P. (2003). Spin entropy as the likely source of enhanced thermopower in NaxCo2O4. *Nature*, 423, 425-428.

[38] Androulakis, J., Migiakis, P. and Giapintzakis, J. (2004). La0.95Sr0.05CoO3: An efficient room-temperature thermoelectric oxide. *Appl. Phys. Lett.*, 84 (7), 1099-1101.

[39] Terasaki, I. (2006). Novel physics and functions in the layered cobalt oxides from thermoelectricity to ferromagnetism. *Physica B*, 383 (1), 107-110.

[40] Taskin, A. A., Lavrov, A. N. and Ando, Y. (2006). Origin of the large thermoelectric power in oxygen-variable RBaCo2O5+x (R=Gd,Nd). *Phys. Rev. B*, 73 (12), 121101/1-121101/4.

[41] Muta, H., Kurosaki, K. and Yamanaka, S. (2004). Thermoelectric properties of doped BaTiO3-SrTiO3 solid solution. *J. Alloys Compd.*, 368, 22-24.

[42] Okuda, T., Nakanishi, K., Miyasaka, S. and Tokura, Y. (2001). Large thermoelectric response of metallic perovskites: Sr1-xLaxTiO3 ($0 < x < 0.1$). *Phys. Rev. B*, 63, 113104/1-113104/4.

[43] Obara, H., Yamamoto, A., Lee, C.-H., Kobayashi, K., Matsumoto, A. and Funahashi, R. (2004). Thermoelectric Properties of Y-Doped Polycrystalline SrTiO3. *Jpn. J. Appl. Phys.*, 43, L540-542.

[44] Ohta, S., Nomura, T., Ohta, H. and Koumoto, K. (2005). High-temperature carrier transport and thermoelectric properties of heavily La- or Nb-doped SrTiO3 single crystals. *J. Appl. Phys.*, 97, 034106/1-034106/4.

[45] Lee, K. H., Kim, S. W., Ohta, H. and Koumoto, K. (2006). Ruddlesden-Popper phases as thermoelectric oxides: Nb-doped SrO(SrTiO3)n (n = 1, 2). *J. Appl. Phys.*, 100, 063717/1-063717/7.

[46] Lee, K. H., Kim, S. W., Ohta, H. and Koumoto, K. (2007). Thermoelectric properties of layered perovskite-type (Sr1-xCax)3(Ti1-yNby)2O7. *J. Appl. Phys.*, 101, 083707/1-083707/6.

[47] Cui, Y., Salvador, J. R., Yang, J., Wang, H., Amow, G. and Kleinke, H. (2009). Thermoelectric properties of heavily doped n-type $SrTiO_3$ bulk materials. *J. Electr. Mater.*, 38, 1002-1007.

[48] Sofo, J. O. and Mahan, G. D. (1994). Optimum band gap of a thermoelectric material. *Phys. Rev. B*, 49, 4565-4570.

[49] DiSalvo, F. J. (1999). Thermoelectric cooling and power generation. *Science*, 285, 703-706.

[50] Mott, N. F. and Jones, H. (1958). *The Theory of the Properties of Metals and Alloys*, New York, NY: Dover Publications.

[51] Mahan, G. D. and Sofo, J. O. (1996). The best thermoelectric. *Proc. Natl. Acad. Sci. USA*, 93, 7436-7439.

[52] Rao, A., Ji, X. and Tritt, T. M. (2006). Properties of Nanostructured One-Dimensional and Composite Thermoelectric Materials. *Mat. Res. Bull.*, 31, 218-223.

This page intentionally left blank.

DOCUMENT CONTROL DATA

(Security markings for the title, abstract and indexing annotation must be entered when the document is Classified or Designated)

1. ORIGINATOR (The name and address of the organization preparing the document. Organizations for whom the document was prepared, e.g. Centre sponsoring a contractor's report, or tasking agency, are entered in section 8.)

Defence Research and Development Canada – Atlantic
9 Grove Street
P.O. Box 1012
Dartmouth, Nova Scotia B2Y 3Z7

2a. SECURITY MARKING (Overall security marking of the document including special supplemental markings if applicable.)

UNCLASSIFIED

2b. CONTROLLED GOODS

(NON-CONTROLLED GOODS)
DMC A
REVIEW: GCEC DECEMBER 2013

3. TITLE (The complete document title as indicated on the title page. Its classification should be indicated by the appropriate abbreviation (S, C or U) in parentheses after the title.)

Advanced materials for soldier power applications through waste-heat recovery: Final report

4. AUTHORS (last name, followed by initials – ranks, titles, etc. not to be used)

Amow, G.

5. DATE OF PUBLICATION (Month and year of publication of document.)	6a. NO. OF PAGES (Total containing information, including Annexes, Appendices, etc.)	6b. NO. OF REFS (Total cited in document.)
September 2009	52	52

7. DESCRIPTIVE NOTES (The category of the document, e.g. technical report, technical note or memorandum. If appropriate, enter the type of report, e.g. interim, progress, summary, annual or final. Give the inclusive dates when a specific reporting period is covered.)

Technical Report

8. SPONSORING ACTIVITY (The name of the department project office or laboratory sponsoring the research and development – include address.)

Defence Research and Development Canada – Atlantic
9 Grove Street
P.O. Box 1012
Dartmouth, Nova Scotia B2Y 3Z7

9a. PROJECT OR GRANT NO. (If appropriate, the applicable research and development project or grant number under which the document was written. Please specify whether project or grant.)	9b. CONTRACT NO. (If appropriate, the applicable number under which the document was written.)
Land Sustain Thrust 12sz	

10a. ORIGINATOR'S DOCUMENT NUMBER (The official document number by which the document is identified by the originating activity. This number must be unique to this document.)	10b. OTHER DOCUMENT NO(s). (Any other numbers which may be assigned this document either by the originator or by the sponsor.)
DRDC Atlantic TR 2009-213	

11. DOCUMENT AVAILABILITY (Any limitations on further dissemination of the document, other than those imposed by security classification.)

Unlimited

12. DOCUMENT ANNOUNCEMENT (Any limitation to the bibliographic announcement of this document. This will normally correspond to the Document Availability (11). However, where further distribution (beyond the audience specified in (11) is possible, a wider announcement audience may be selected.))

Unlimited

13. ABSTRACT (A brief and factual summary of the document. It may also appear elsewhere in the body of the document itself. It is highly desirable that the abstract of classified documents be unclassified. Each paragraph of the abstract shall begin with an indication of the security classification of the information in the paragraph (unless the document itself is unclassified) represented as (S), (C), (R), or (U). It is not necessary to include here abstracts in both official languages unless the text is bilingual.)

With the ever increasing power demands required for the dismounted soldier, ongoing efforts have been underway to identify alternatives to battery use. Emerging technologies such as fuel cells show promise for increased power densities and thus have the potential for reducing footprint and enabling longer mission times, whilst thermoelectric devices can convert the waste heat into useable power from various sources such as that produced by fuel cells and natural body heat.

This report describes the most significant results of a three year Technology Investment Fund (TIF) project focused on addressing materials issues related to solid-oxide fuel cells and thermoelectric materials. Namely, the development of a novel porous electrolyte supported solid oxide fuel cell (SOFC) architecture and the development of novel materials for SOFC cathodes, thermoelectric oxides and polymers.

En raison des demandes de puissance électrique de plus en plus grandes pour l'infanterie débarquée, on continue de déployer des efforts dans le but de trouver des solutions de remplacement aux piles. Certaines technologies émergentes, comme les piles à combustible, s'avèrent intéressantes pour obtenir une densité de puissance accrue et ont, par le fait même, le potentiel de réduire l'empreinte et d'effectuer des missions plus longues; les dispositifs thermoélectrique peuvent, quant à eux, convertir la chaleur dissipée en puissance utilisable à partir de différentes sources, comme la chaleur produite par les piles à combustible et la chaleur naturelle du corps.

Le présent rapport décrit les résultats les plus significatifs d'un projet de Fonds d'investissement technologique (FIT) d'une durée de trois ans. Le projet portait sur des questions pratiques liées aux piles à combustible à oxyde solide (SOFC, de l'anglais *Solid Oxide Fuel Cell*) et aux matériaux thermoélectriques. Plus précisément, on procédera à l'élaboration d'une nouvelle architecture de pile à combustible à oxyde solide à support électrolytique poreux et de nouveaux matériaux pour les cathodes de SOFC, les oxydes thermoélectriques et les polymères.

14. KEYWORDS, DESCRIPTORS or IDENTIFIERS (Technically meaningful terms or short phrases that characterize a document and could be helpful in cataloguing the document. They should be selected so that no security classification is required. Identifiers, such as equipment model designation, trade name, military project code name, geographic location may also be included. If possible keywords should be selected from a published thesaurus, e.g. Thesaurus of Engineering and Scientific Terms (TEST) and that thesaurus identified. If it is not possible to select indexing terms which are Unclassified, the classification of each should be indicated as with the title.)

Dismounted soldier, Power and energy, fuel cells, thermoelectric, waste heat recovery, novel materials

Defence R&D Canada

Canada's Leader in Defence
and National Security
Science and Technology

R & D pour la défense Canada

Chef de file au Canada en matière
de science et de technologie pour
la défense et la sécurité nationale

www.drdc-rddc.gc.ca